Journal of Environmental Radioactivity 190–191 (2018) 51–65

Contents lists available at ScienceDirect

Journal of Environmental Radioactivity

journal homepage: www.elsevier.com/locate/jenvrad

Calibration of Safecast dose rate measurements

Guido Cervone[a,b,*], Carolynne Hultquist[a]

[a] Geoinformatics and Earth Observation Laboratory, Dept. of Geography and Institute for CyberScience, The Pennsylvania State University, University Park, PA, United States

[b] Research Application Laboratory, National Center for Atmospheric Research, Boulder, CO, United States

ARTICLE INFO

Keywords:
Safecast data
Data calibration
Volunteered geographic information
Citizen science
Fukushima Daiichi

ABSTRACT

A methodology is presented to calibrate contributed Safecast dose rate measurements acquired between 2011 and 2016 in the Fukushima prefecture of Japan. The Safecast data are calibrated using observations acquired by the U.S. Department of Energy at the time of the 2011 Fukushima Daiichi power plant nuclear accident.

The methodology performs a series of interpolations between the U.S. government and contributed datasets at specific temporal windows and at corresponding spatial locations. The coefficients found for all the different temporal windows are aggregated and interpolated using quadratic regressions to generate a time dependent calibration function. Normal background radiation, decay rates, and missing values are taken into account during the analysis.

Results show that the standard Safecast static transformation function overestimates the official measurements because it fails to capture the presence of two different Cesium isotopes and their changing magnitudes with time. A model is created to predict the ratio of the isotopes from the time of the accident through 2020. The proposed time dependent calibration takes into account this Cesium isotopes ratio, and it is shown to reduce the error between U.S. government and contributed data. The proposed calibration is needed through 2020, after which date the errors introduced by ignoring the presence of different isotopes will become negligible.

1. Introduction

Safecast is a widespread Volunteered Geographic Information (VGI) project started in the immediate aftermath of the 2011 Japanese nuclear emergency to collect spatio-temporal radiation dose rate measurements (Safecast, 2016). It relies on “citizens as sensors” (Goodchild, 2007) to collect distributed data and upload them to a central open access repository. VGI refers to datasets which are voluntarily contributed, and contain temporal and spatial information (Fast and Rinner, 2014). Because of the massive amount of real-time, on-the-ground data generated and distributed daily, the utilization of VGI during emergencies is a new and growing area of research (Cervone et al., 2016a).

Citizen-led movements aimed at measuring environmental variables could generate actionable data for situational awareness during emergencies (Sprake and Rogers, 2014). Sensors for environmental data collection are being built using inexpensive off-the-shelf components (Hemmi and Graham, 2014). The widespread use of mobile devices, paired with the increased reliability and speed of wireless networks, enable citizens to share data reliably and in real-time (Cervone et al., 2016b). However, despite the availability of massive contributed geospatial ‘big data’, they are often not validated in a rigorous setting and by an independent set of researchers. Because of this lack of verification, crowdsourced data are usually not considered reliable for use during emergencies despite their suitability (Fairbairn and Al-Bakri, 2013; Fowler et al., 2013). If properly validated, citizen science projects could provide actionable data during emergencies (Sprake and Rogers, 2014).

1.1. Prior research using Safecast data

Despite the large number of active users and massive quantity of observations collected, Safecast data received limited external scientific validation from researchers. An initial study by Coletti et al. (2017) performed statistical tests to compare about five weeks of Safecast data (2011-04-23 to 2011-05-30) with U.S. government measurements over an area of approximately 100 km^2 in the Fukushima prefecture. They concluded that Safecast data are correlated with the government measurements, but that the distributions of the two datasets are different. They showed that the DOE/NNSA observations were generally

* Corresponding author. Geoinformatics and Earth Observation Laboratory, Dept. of Geography and Institute for CyberScience, The Pennsylvania State University, University Park, PA, United States.

E-mail addresses: cervone@psu.edu (G. Cervone), hultquist@psu.edu (C. Hultquist).

https://doi.org/10.1016/j.jenvrad.2018.04.018
Received 17 August 2017; Received in revised form 18 April 2018; Accepted 19 April 2018

higher than the corresponding Safecast values, but this result is true only on a rather small subset of the data used in their study. Successive studies using additional data showed that Safecast tend to over-estimate the DOE dose rate measurements.

A study by Hultquist and Cervone (2017) compared 5 years of Safecast data with official measurements. Both DOE and Safecast data were decay corrected to allow for comparison at specific dates and then spatially standardized after data was aggregated to a common grid. Decay corrected DOE data were compared to raw Safecast data collected within a fixed temporal window. The results showed a high correlation between the two datasets, but also a systematic bias (over-estimation) in the Safecast data. Spatio-temporal maps were created to compare Safecast data collected within a month long temporal window with U.S. government measurements that were corrected for decay for the middle of the same month. The maps in this study showed an overall good correlation. However, no tests were performed specifically to characterize or try removing this bias from the Safecast data.

This research presents a methodology to characterize the bias, and proposes a time dependent mathematical function to remove this bias from the Safecast data. The calibration method described is applicable both to previously collected data, as well as to data that will be collected in the future. Calibrated Safecast data could be used during emergencies to complement government measurements or provide an assessment when other sources of data are not available.

1.2. Fukushima Daiichi nuclear accident

On 2011-03-11 at 05:46 UTC (14:46 local time, UTC +9) a massive Mw 9.0 underwater earthquake occurred 70 km offshore of the eastern coast of Japan, with the epicenter at 38.322N and 142.369E. The earthquake generated a tsunami that rapidly hit the eastern coast of Japan, and propagated across the Pacific Ocean. A tsunami wave hit the Fukushima Daiichi Nuclear Power Plant (FDNPP) about 40 min after the earthquake which led to a cooling system dysfunction.

Several radioactive releases ensued as a result of an increase of pressure and temperature in the nuclear reactor buildings. Some releases were the result of both controlled and uncontrolled venting, while others were the result of explosions that compromised the containment structures. The explosions were most likely caused by ignited hydrogen, generated by reaction between zirconium and water occurring after the reactor core damage. Several radioactive isotopes were released into the environment, and of particular importance for this research are the releases of Cesium, and more specifically ^{137}Cs and ^{134}Cs isotopes with a half-life of approximately 30 and 2 years respectively. Other radioactive elements released have a much shorter half-life (e.g. Iodine or Zirconium; in the order of hours to days), that quickly decay and thus can be omitted from the computations (Morino et al., 2011).

The largest radioactive emissions occurred between the 2011-03-12 and 2011-03-21. Radioactive particles were quickly transported regionally which contaminated several areas of Japan and traces of the release reached North America and Europe (Bowyer et al., 2011; Potiriadis et al., 2011; Masson et al., 2011). Elevated levels of radiation were recorded at different locations throughout Japan on the ground, in the water, and in the air. The individual radionuclide distributions assessed by Kinoshita et al. (2011) over central-east Japan and starting at the FDNPP nuclear power plant indicate that the prefectures of Fukushima, Ibaraki, Tochigi, Saitama, and Chiba and the city of Tokyo had higher than normal radiation dose rates due to the dispersed radioactive elements.

Estimating the fate of the contaminants and predicting their health impact quickly became an issue of great importance (Calabrese, 2011). Transport and dispersion (T&D) models were used to compute radioactivity levels and ground deposition, as well as to estimate the non-steady source release for the accident (Yasunari et al., 2011; Stohl et al., 2012; Terada et al., 2012; Katata et al., 2012; Cervone and Franzese, 2014). At the same time, the Safecast project was started to monitor radiation levels on the ground, and to provide an independent assessment of the emergency.

2. Data

This study is based on radiation data from a U.S. Department of Energy (DOE) survey, contributed volunteered measurements (Safecast), nine deposition studies from the Japan Atomic Energy Agency (JAEA), and a background radiation survey from the Japanese National Institute of Advanced Industrial Science and Technology (AIST). Additionally, elevation data from the Advanced Spaceborne Thermal Emission and Reflection (ASTER) satellite were also used, mainly for plotting purposes.

2.1. Background radiation

The AIST completed a 2007 survey of natural background radiation. The data covers the majority of Japan at a resolution of about half a kilometer and captures the natural variation in the background radiation, which for the most part, is dependent on the local topography and geology. In this research, the term anomaly is used to refer to the transformed radiation observations (both U.S. government and Safecast), where the spatially corresponding natural occurring background radiation has been subtracted from each measurement. The resulting anomaly is assumed to represent the increase in radiation caused by the Fukushima nuclear accident.

Fig. 1 (a) shows the background radiation for most of Japan, with values ranging from between 0.05 and 0.30 μSv/h. The study area, defined by the convex hull that encompasses the available DOE radiation data, is shown in hashed red. Fig. 1 (b) shows the background radiation for the study area, with values ranging between 0.06 and 0.16 μSv/h. The extent of the DOE measurements (shown in red) corresponds to the edge of the polygon, and is used in all maps to mask the study area. The figure also shows the location of the FDNPP which is indicated with a red diamond at 37.4213N, 141.0331E. Additionally, concentric arcs are plotted at 20, 40, and 60 km from the power plant. The locations of the power plant and the arcs are included in all maps for reference and to ease the visual comparisons.

2.2. JAEA surveys

The JAEA took surveys of the energy spectrum of gamma-ray emitting radioactive nuclides (Saito et al., 2015). The Cesium deposition density surveys during the period ranging from 2011-04-29 to 2013-03-11 are interpolated and distributed as raster datasets with a spatial cell resolution of 500 m^2 (Japan Atomic Energy Agency, 2014). Fig. 2 shows the ratio of ^{134}Cs over (^{137}Cs + ^{134}Cs) for the nine surveys performed. Note that the extents of the surveys are not consistent but there is a significant overlap. The color scale is identical for all figures, and shown in the last panel. The ratio monotonically decreases as a function of time because of the shorter half-life of ^{134}Cs with respect to ^{137}Cs. While there are spatial variations over the domain, the range of values is small and overall consistent, regardless of the domain extent. The figure shows an average starting ratio of approximately 0.5 in 2011, which is consistent with the published source term parameters of the nuclear release, and an average ratio of approximately 0.3 in 2013.

2.3. DOE data

The DOE in conjunction with the U.S. National Nuclear Security Administration (NNSA) responded to the accident by running a number of missions to acquire airborne remote sensing radiation levels in the Fukushima prefecture between 2011-03-14 and 2011-05-28 (Lyons and Colton, 2012). The data provide a broad footprint of the radiological release over land, and are assumed to be the 'ground truth' for this

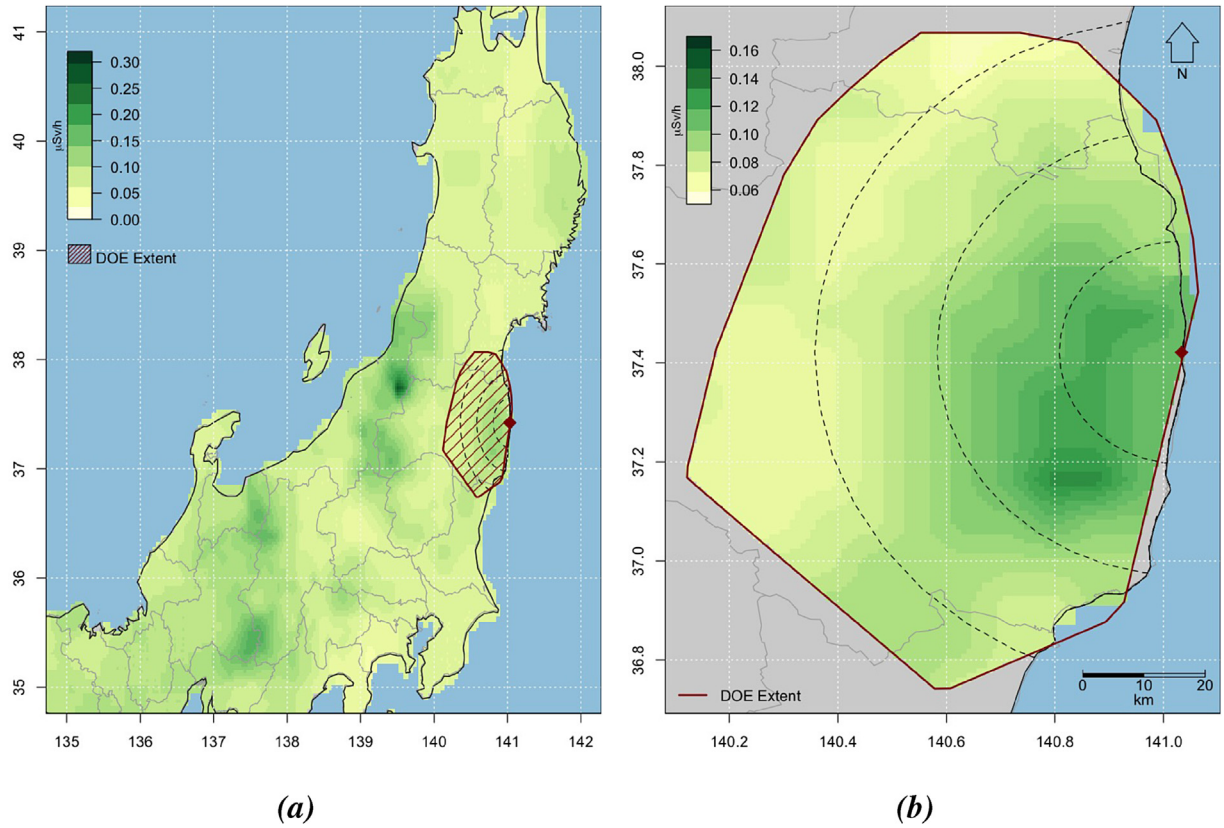

Fig. 1. Natural background radiation level for most of Japan (a) and with a subset of the study area (b).

study.

The dose rate measurements were collected by the United States Aerial Measuring System (AMS) with large thallium activated sodium iodide NaI(Tl) crystals using fixed-wing and rotary-wing aircrafts over broad swaths and following a standard pattern. The AMS survey flights were flown for the fixed-wing airplanes at $72ms^{-1}$ (140 knots) with an altitude of 550–700 m above ground at 610–1610 m line spacing while the helicopters were flown at $36ms^{-1}$ (70 knots) 152–305 m above ground with 305–610 m line spacing (Lyons and Colton, 2012). The release of radioactive materials occurred over complex terrain and lasted over multiple days.

Using air attenuation coefficients, the gamma count rates measured at an altitude were extrapolated to an exposure rate 1 meter above the ground and subsequently ground-truthed along test lines (Lyons and Colton, 2012). It is assumed that this method, when performed correctly, transforms the aerial measurements to a corresponding 1 meter above-ground exposure rate equivalent.

The DOE/NNSA (ensuing referred only as DOE) provides a publicly available set of above-ground exposure rates. The public dataset contains over 107,000 observations that cover roughly 13,000 km^2 in the Fukushima prefecture and were collected for a period of 5 weeks from 2011-04-02 through 2011-05-09 (Department of Energy, 2011). The U.S. Government data were released after being corrected for decay to the date of 2011-06-30 with ^{134}Cs and ^{137}Cs isotopes assumed at a 1:1 (0.5) ratio. In order to simplify the computation, the DOE data were decay corrected to 2011-04-15 to cover the full temporal range of available Safecast data. While it is known that applying a decay correction in a reverse manner is not a generally accepted practice, it is permissible in this study because the temporal range for this operation is very small compared to the overall length of the study, and furthermore, the date of interest is within the time range of when the data were collected.

Fig. 3 (a) shows the DOE measurements in vector format in μSv/h and in log10 scale. The scale and color scheme are kept consistent throughout the maps and figures to allow for an easy comparison. There is a distinguishable footprint of increased radiation starting at the power plant, and extending North-West throughout the domain. Fig. 3 (b) shows the DOE measurements rasterized to a 0.5 km^2 grid by taking the maximum value of all the DOE measurements falling within each cell. Additionally, cells with no overlapping measurements were assigned a value using a bilevel linear interpolation if at least 6 of their 8 neighboring cells contained a value. Cell values were not otherwise extrapolated, and this method explains why some cells in the spatial distribution, primarily North and West of the domain, do not contain values.

Fig. 3 (c) shows the rasterized DOE data after removing the normally occurring background radiation (see Fig. 1 (a)). Specifically, the figure only shows values that are larger than 0.001 μSv/h (1E-2 in the log10 scale), which corresponds to about 10% of the background radiation for the study area. This definition of a lower bound is made to compensate for measurements and rounding errors, and it is applied to all computations. The figure shows the anomaly (values above background), which is assumed to be caused by the nuclear accident releases. Fig. 3 (d) shows a Digital Elevation Model (DEM) for the study area retrieved from the NASA ASTER satellite. The DEM has a spatial resolution of 30 m and a vertical resolution in the order of a few cm, depending on slope and land cover. The elevation ranges from sea level to about 2500 m North-West of the study area. The extent of the radiation anomaly is shown in opaque red. The figure shows that the anomaly follows the terrain, and spreads South-West through the valley bounded by the high mountains to the West.

The anomaly shown in Fig. 3 (c), is assumed to be the ground truth, and is the distribution used to calibrate the Safecast data. It is important to note that implicit to the DOE AMS data are uncertainties, however the goal of this research is not to validate or improve on this data set, but to determine if it is possible to gain a comparable distribution using

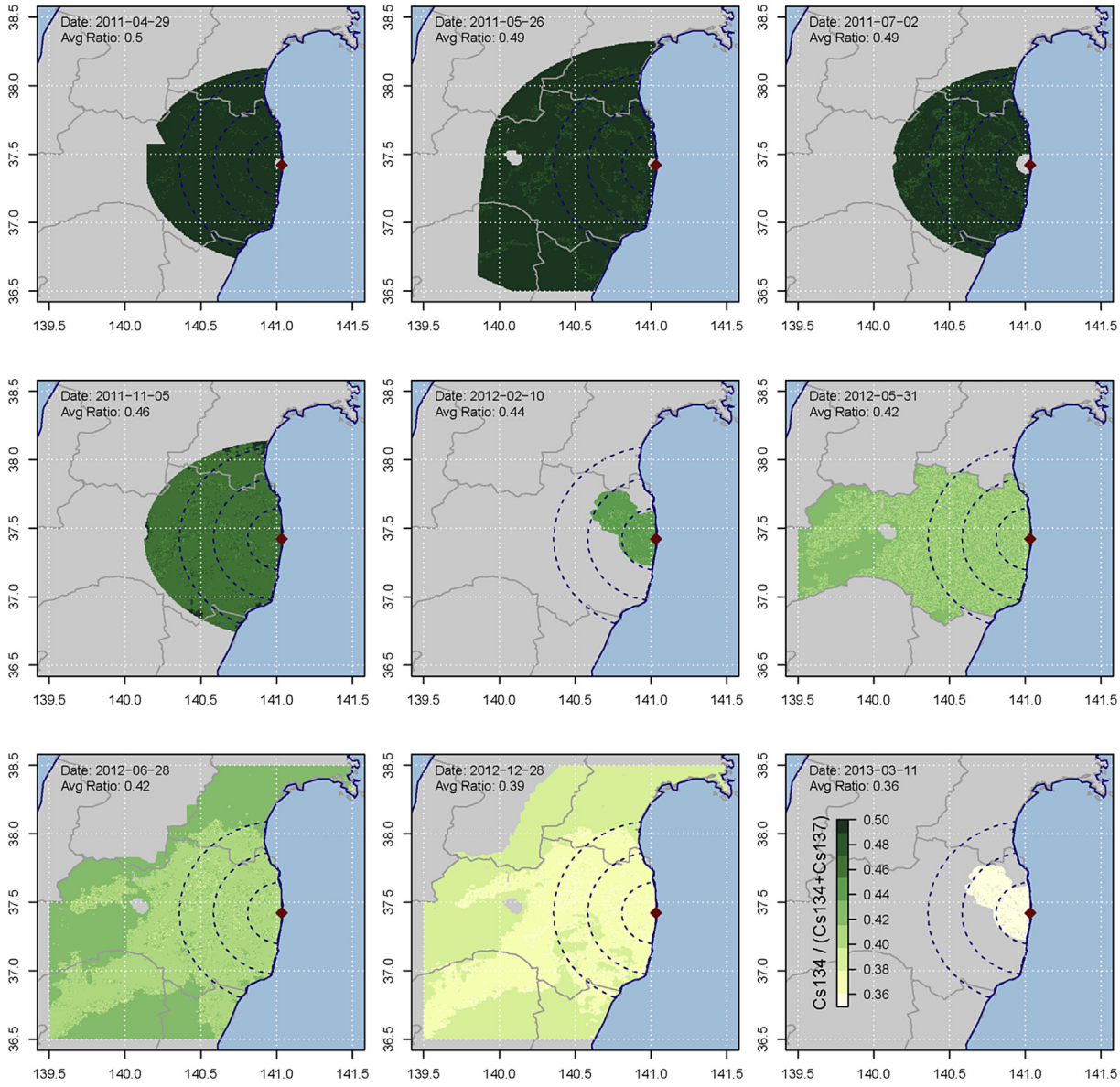

Fig. 2. Field study results showing the ratio of ^{134}Cs over (^{137}Cs + ^{134}Cs) observed from airborne surveys between April 2011 and March 2013.

Safecast data. In an emergency response situation, aerial gamma survey data may be used to make decisions. If distributions gained from Safecast data are comparable, the data could be used to provide additional quick response information about the extent of radiological contamination.

2.4. Safecast data

The Safecast dose rate measurements are acquired using inexpensive Geiger counters that can be purchased as a kit or already assembled (Safecast, 2015b). Measurements are collected every five seconds and are geolcated through satellite Global Positioning System (GPS). The data are streamed through the use of Bluetooth or uploaded manually through a central repository of data. The data are freely available and can be downloaded through the Safecast website, or through the use of a public Application Programming Interface (API) (Brown et al., 2016a). As of December 2016 there were over 60 million logged observations from around the globe, with about 70% of them originating in Japan, primarily in Fukushima, surrounding prefectures, and in major Japanese cities (Brown et al., 2016a). Up until 2013, the greatest majority of the measurements were confined to Japan, but worldwide measurements have been more frequent ever since and improved the global coverage. Safecast is currently a global project with participants collecting data in over 100 countries.

The Safecast data are acquired using bGeigie Nano Geiger counters developed as cost effective devices for monitoring ionizing radiation particles. The bGeigie Nano can be bought online as a kit designed with off-the-shelf parts. It uses the widely used and accurate LND7317 pancake sensor, a Geiger-Müller tube that is sensitive to gamma, beta, and alpha radiation. The device is however shielded from alpha rays, and it has a separate setup for the monitoring of just beta particles. The bGeigie Nano is preset to monitor radiation from radionuclide ^{137}Cs in Counts Per Minute (cpm). The standard conversion factor used by the Safecast community to convert from cpm to μSv/h is thus based only on the observed ^{137}Cs contribution, and is shown in Equation (1).

$$1\,\mu Sv/h = \frac{1}{334} cpm \tag{1}$$

A quality control process is implemented to ensure equipment accuracy of the sensor at the factory (Safecast, 2015a). In addition, a sample of assembled devices are independently tested at centers in Germany, Austria, and the U.S. The tested units have demonstrated

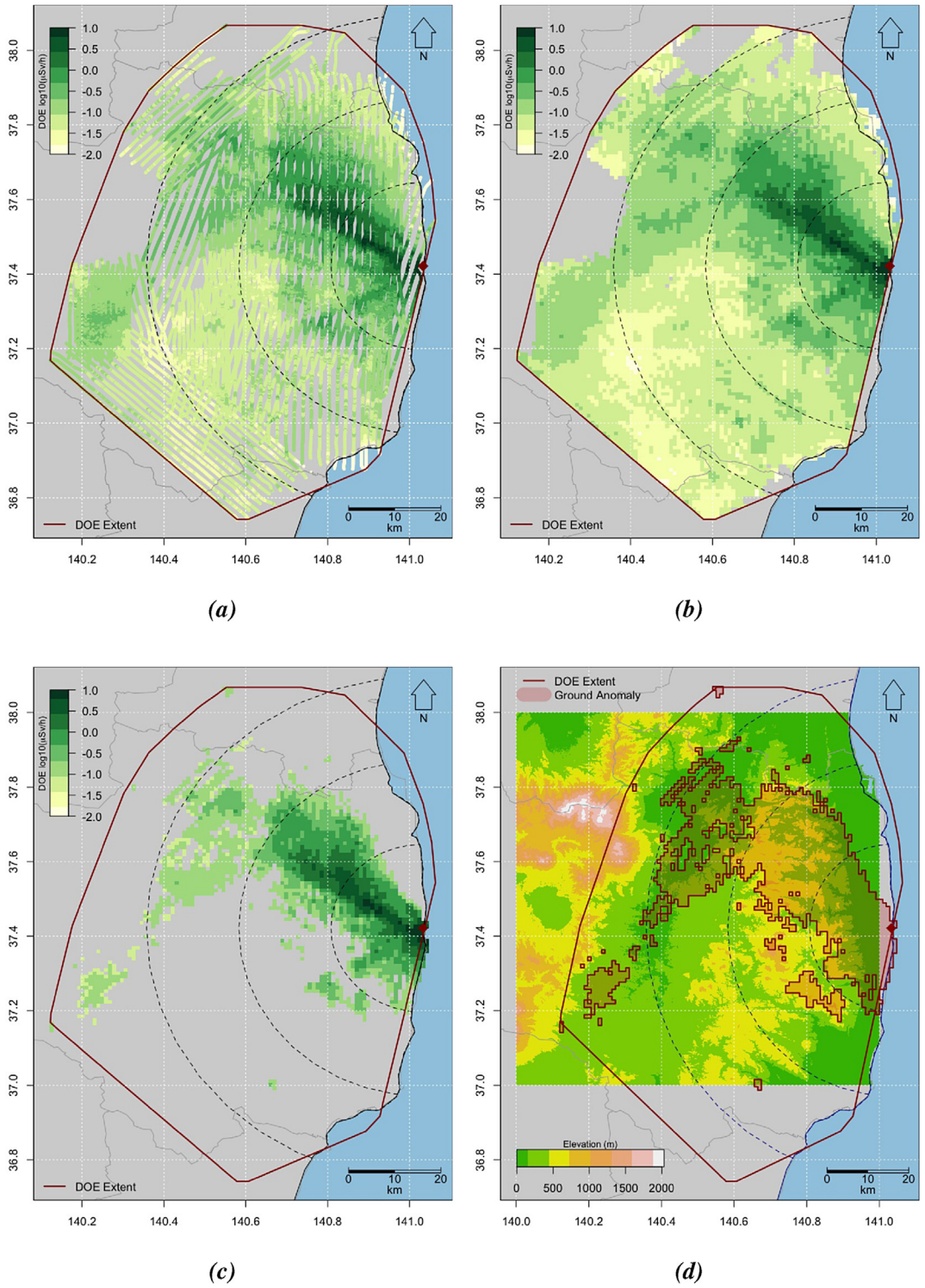

Fig. 3. Original DOE data in vector format (a); rasterized DOE data (b); anomaly defined as the rasterized DOE data minus the background (c); footprint of the anomaly over the DEM of the area (d).

± 10% accuracy, which is consistent with the normal accuracy of industry standards for calibration (Spinrad, 2011). Finally, all data uploads are checked by the Safecast team before being accepted into the database (Brown et al., 2016b).

The Safecast Geiger counters have a flash memory card to store observations, a Bluetooth connection for data transfer, and a GPS receiver to record the location of the observations. The measurements are freely available through either a website or the API. Safecast data are available from about two weeks after the nuclear release and are currently being uploaded by an active community of volunteers. For this research paper, Safecast data are used from 2011-04-24 13:29:26 JST (Japan Standard Time) through 2016. This research only considers Safecast measurements in the study area bounded by the available DOE data and that is collected at about 1 meter above ground level.

Fig. 4 (a) shows the location and number of Safecast observations used in this study, plotted in log10 scale, after rasterizing the data to the same grid used for DOE. Some cells contain as many as one hundred thousand observations, which correspond to highly populated areas,

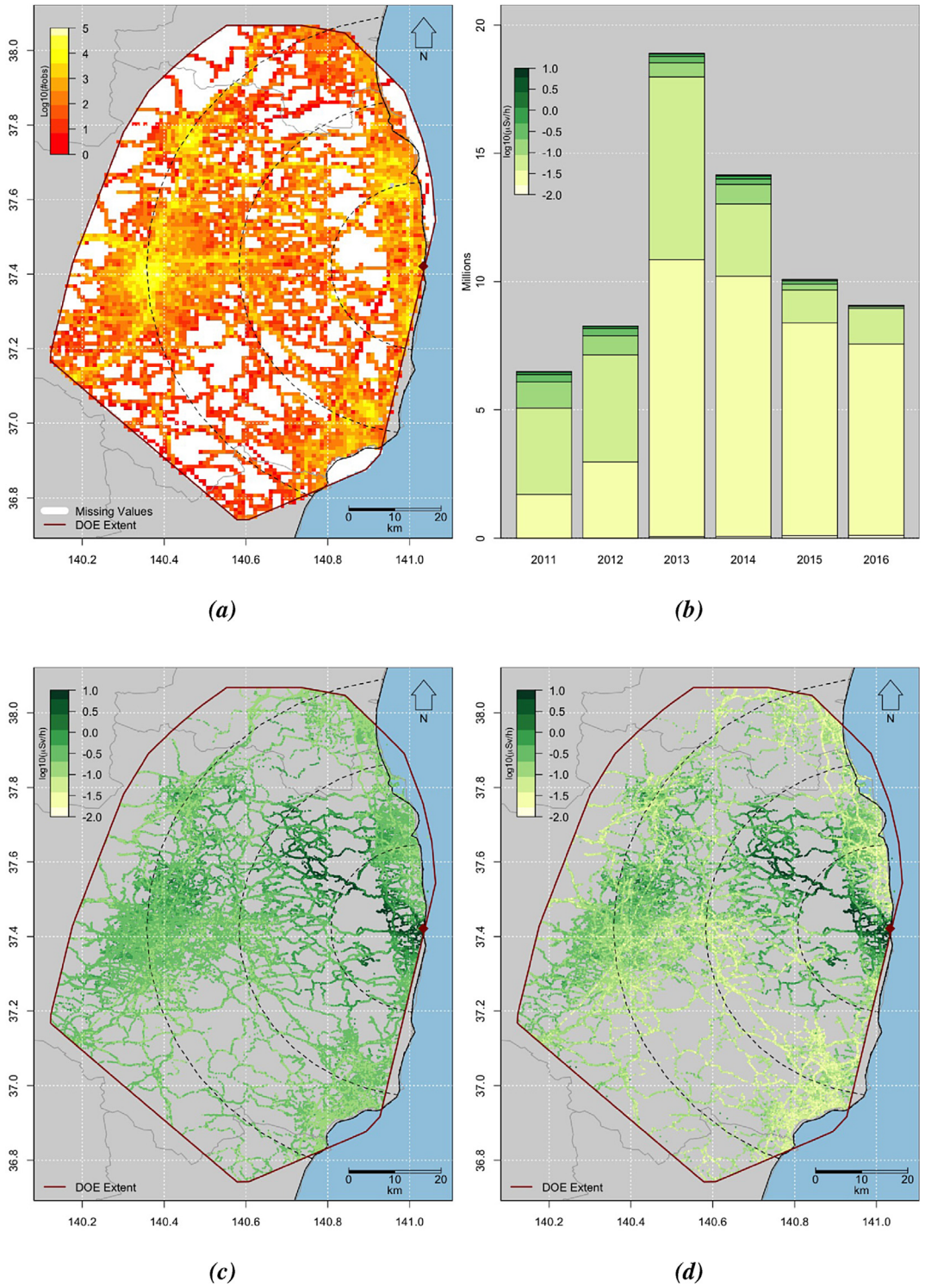

Fig. 4. Number of Safecast measurements over the study area (a); number of measurements aggregated by year and by dose rate (b); original Safecast data in raster format (c); rasterized Safecast data minus the background radiation level (d).

while others contain less than ten observations. Missing data are shown in white, indicating that no Safecast observations are available within the grid cell. Fig. 4 (b) shows the number of the Safecast measurements aggregated by year and stacked by radiation level. The peak number of measurements was reached in 2013, with nearly two million measurements, while the smallest number was acquired in 2011, with about 600,000. In 2016 about 900,000 measurements were made. This trend is relative only to the study area, and it is different when compared with the amount of data acquired over the entire of Japan or worldwide. The figure shows that most measurements are less than 0.1 μSv/h, which is equivalent to the average of the background in the study area (See Fig. 1 (b)). A comparatively smaller number of measurements are available with values higher than 1 μSv/h, related to the radiation anomaly. The highest value recorded is 234.75 μSv/h, recorded within the FDNPP facility at location (37.42144 N, 141.0319 E) on 2015- 05-18 07:18:24 JST. A total of 19,358 measurements above ten μSv/h are recorded in this space and time subset of the data.

Fig. 4 (c) are the original Safecast data in raster format and (d) the

same after removing the background. The Safecast data show consistently higher values than the corresponding DOE data (Fig. 3 (bottom right)). The higher dose rates in the raw data are due to a lack of proper conversion from CPM to μSv/h which takes into account the varying ratio of the Cesium isotopes.

2.5. Data rasterization

All data used in this study are rasterized using the same grid of 137 rows by 99 columns, for a total of 13,563 cells. Each cell has a resolution of 0.5 km^2, and the extent is between latitude 36.74472N and 38.06909N, and longitude 140.1202E and 141.0672E. The rasterization is performed by assigning each point to a grid cell, and then applying a function (mean for Safecast and maximum for DOE) to all points within the cell. Points that fall on a cell border are placed in the cell to the right or below.

3. Methodology

The proposed methodology is based on an iterative algorithm that:

1. Performs decay correction of the entire DOE data and the Safecast data for a specific temporal window to a specific date.
2. Performs linear regression to characterize the bias in the decay corrected Safecast data for this temporal window with respect to the decay corrected DOE data.
3. Creates a general function that characterizes the trend in the linear regressions performed over multiple extending temporal windows.
4. Applies the calibration to the entire Safecast dataset and quantifies the overall error.

Fig. 5 describes the operations (rectangles) and the data (cylinders) used in the method proposed, each being uniquely color coded. The AIST data (green) are used to compute the background for the study area. DOE raw data (yellow) are used to define the study area, and then compute the anomaly after removing the background from each measurement. The individual measurements are then rasterized to create the gridded anomaly that is used in all the computations.

The Safecast data are pre-processed by first clipping them to the extent for which DOE data exist, then changing the unit from cpm to μSv/h, and finally computing the anomaly by removing the normal background level from each observation. The JAEA data are used to identify the ratio of Cesium isotopes as a function of time, which must be known in order to properly correct the data for decay.

The large grey dashed rectangle shows operations that are repeated for different temporal subsets, called temporal windows, each ranging from the begin of the data (2011-04-24) to a specific date. The temporal windows are necessary for Safecast data because they are a data stream being continuously collected. The U.S. government DOE measurements are static and were collected at the time of the March 2011 FDNPP accident.

The Safecast data are first temporally subsetted by disregarding all data occurring after a specified date, unless the entire data are used. They are then decay corrected using the time dependent Cesium ratio for this temporal window, and gridded to the same common grid. The DOE data are also decay corrected using the same Cesium ratio. Finally, a linear regression is performed between each corresponding grid cell of the rasterized and decay corrected Safecast and DOE data.

The decay correction of the DOE data consists in correcting each grid cell for decay, and is a quick process because there are a maximum of 13,563 cells, out of which several have missing values or contain values below background. In this case study, the number of valid grid cells is only 15% circa of the total number of grid cells. In the case of Safecast, the decay correction is computed for each individual measurements above background that was collected during a specific temporal window. While this could potentially be a very computationally expensive task because of the presence of millions of Safecast observations, similarly to the case for DOE data, the number of values above background is a smaller portion of the total number of available measurements.

The Safecast values, that are still above background levels after the decay corrected operations are performed, are rasterized to the same

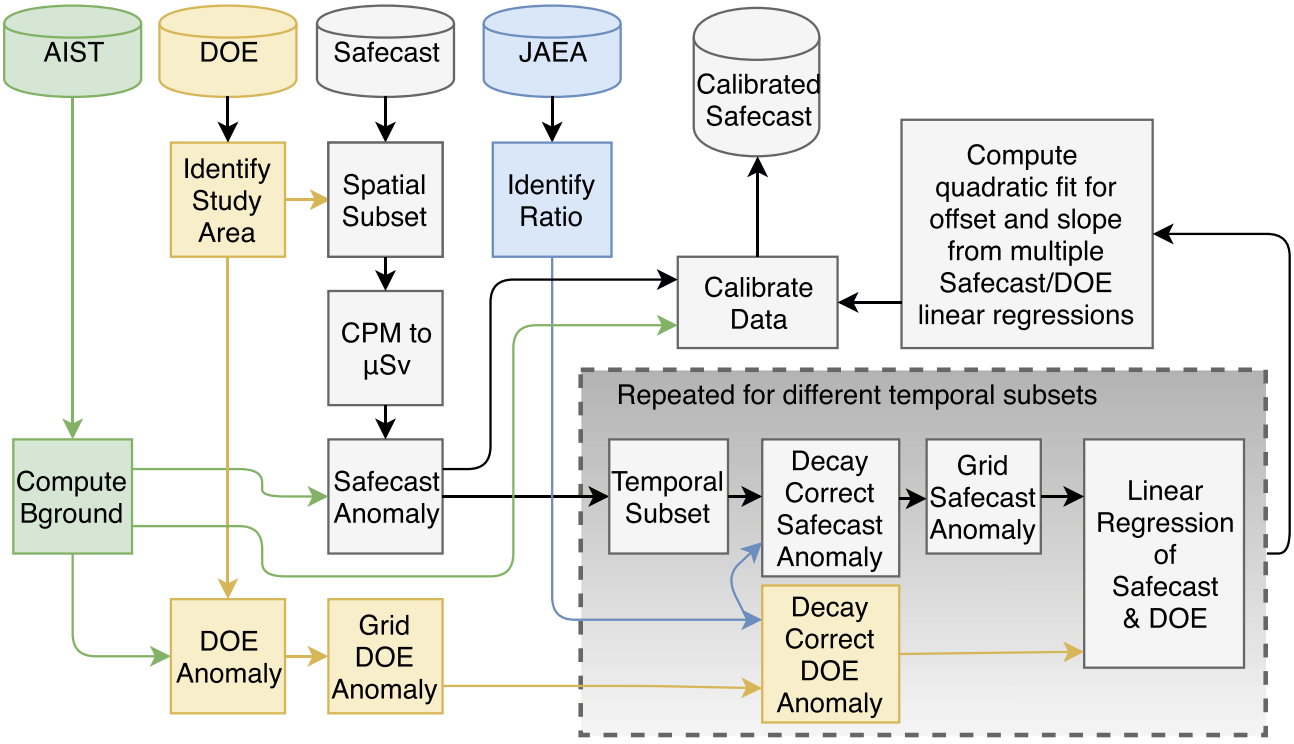

Fig. 5. Flowchart of the methodology developed to calibrate Safecast to DOE using a quadratic fit from multiple linear regressions.

Table 1
Unit decay and numerical prediction for the ratio of ^{134}Cs and ^{137}Cs isotopes as a function of time. Time is shown as the number of seconds since the start of the accident.

ID	^{134}Cs Unit Decay	^{137}Cs Unit Decay	Elapsed Days	Dates	R_t
1	1.00	1.00	1	2011-03-15	0.50
2	0.97	1.00	47	2011-04-30	0.49
3	0.89	0.99	170	2011-08-31	0.47
4	0.81	0.99	292	2011-12-31	0.45
5	0.73	0.98	413	2012-04-30	0.43
6	0.64	0.98	536	2012-08-31	0.40
7	0.56	0.97	658	2012-12-31	0.37
8	0.49	0.96	778	2013-04-30	0.34
9	0.45	0.96	901	2013-08-31	0.32
10	0.41	0.95	1023	2013-12-31	0.30
11	0.37	0.95	1143	2014-04-30	0.28
12	0.33	0.94	1266	2014-08-31	0.26
13	0.29	0.94	1388	2014-12-31	0.24
14	0.25	0.93	1508	2015-04-30	0.21
15	0.23	0.93	1631	2015-08-31	0.20
16	0.21	0.92	1753	2015-12-31	0.18
17	0.19	0.92	1874	2016-04-30	0.17
18	0.17	0.91	1997	2016-08-31	0.16
19	0.15	0.90	2119	2016-12-31	0.14
20	0.13	0.90	2239	2017-04-30	0.12
21	0.12	0.89	2362	2017-08-31	0.12
22	0.11	0.89	2484	2017-12-31	0.11
23	0.10	0.88	2604	2018-04-30	0.10
24	0.09	0.88	2727	2018-08-31	0.09
25	0.08	0.87	2849	2018-12-31	0.08
26	0.07	0.87	2969	2019-04-30	0.07
27	0.06	0.86	3092	2019-08-31	0.06
28	0.05	0.85	3214	2019-12-31	0.06
29	0.05	0.85	3335	2020-04-30	0.05
30	0.04	0.84	3458	2020-08-31	0.05
31	0.04	0.84	3580	2020-12-31	0.04

common grid used for all computations. The rasterization of the Safecast data is calculated by taking the average of the observations falling within a grid cell, unlike the DOE case where the maximum was used. Using the average value for Safecast is recommended because the data carry uncertainty, with measurements within a grid cell varying dramatically. On the other hand, DOE data are vetted, and show little variation in the distribution of multiple measurements within a grid cell. By taking the average value of the measurements within a cell the methodology is less sensitive to noise. Additional tests were also performed using the median instead of the mean, and they led to nearly identical results.

The coefficients of the multiple linear regressions performed with varying temporal window sizes are regressed using a quadratic function. The results of the quadratic regression provide a time dependent slope and intercept which are used to calibrate the Safecast data. This quadratic function and its coefficients are the main contributions of this research, and provide a robust way to calibrate Safecast data. After calibrating each Safecast measurement, the background is reintroduced to quantify the total dose rate.

3.1. Unit conversion

Safecast and DOE are measured in different radiation units so conversion to a standard unit is necessary. The Safecast data are measured by Geiger-Müller tubes that record cpm as a count rate of ionizing radiation particles. DOE uses the unit of microsieverts per hour (μSv/h) thus it is necessary to convert to the same unit.

The unitμSv/h is a SI unit of radiation absorbed dose equivalent, and it corresponds to a biological dose. The conversion between cpm to μSv/h is computed using the characteristics of the specific type of radiation. The Safecast dose rate measurements are converted from cpm to μSv/h using the conversion factor shown in Equation (1). The standard Safecast conversion factor assumes that only ^{137}Cs is present, and does not account for the presence of ^{134}Cs. Because the ratio between the two Cesium isotopes varies over time as a result of their different half-lives, an error is introduced when converting from cpm to μSv/h using Equation (1).

3.2. Cesium decay correction

The Safecast and DOE datasets are decay corrected in order to compare them despite their different temporal extents. The decay correction operations described are applied both to each grid value for the DOE data, and to each individual Safecast measurement. The decay of a dose rate is carried out according to Equation (2),

$$D(\delta t, hl) = exp\left(-\left(0.693 \times \frac{\delta t}{T_{1/2}}\right)\right) \tag{2}$$

where δt is the length in years of the decay, and $T_{1/2}$ is the half-life also in years. The decay corrected value D^{tot} for any radiation measurement over any length of time is defined as the sum of the decay corrected relative contribution of each isotope (Equation (3)).

$$D^{tot}(M_t, R_t, \delta t) = (M_t \times (1 - R_t) \times D(\delta t, T_{1/2}^{137})) + (M_t \times R_t \times D(\delta t, T_{1/2}^{134})) \tag{3}$$

where M_t is the initial dose rate at time t in μSv/h from Equation (1), R_t is the ratio of the isotopes at time t, $T_{1/2}^{137}$ is the half-life for ^{137}Cs (30.17 years) and $T_{1/2}^{134}$ is the half-life for ^{134}Cs (2.06 years). The ratio between the Cesium isotopes present is thus fundamental because the isotopes decay at different rates, and the correlation is computed at any time t according to Equation (4).

$$R_t = \frac{^{134}Cs}{^{137}Cs + ^{134}Cs} \tag{4}$$

The ratio R_t at the time the DOE data were collected was estimated to be 0.5. For Safecast data, much of which is collected well after the radioactive release, the ratio of Cesium changes constantly over time, but the actual concentrations of ^{137}Cs and ^{134}Cs over the study domain are known only at specific times when the JAEA field studies were carried out to measure them (Fig. 2).

A model was implemented to predict the ratio R_t of the Cesium isotopes as a function of time by decaying unitary measurements according to their respective half-lives (Table 1). The columns show the unit decay for ^{134}Cs and ^{137}Cs, the date in Gregorian format, and the predicted ratio R_t. The initial release was assumed to occur on 2011-03-14 at 00:00:00 JST, and to have a concentration of one μSv/h for each isotope. Fig. 6 shows the prediction for the ratio R_t and how it compares to the field measurements. Each of the field studies are represented with a boxplot to show the spatial variation over the domain. The only case in which the ratio between the isotopes varies significantly over the domain (about 7%) occurs in the 2012-12-28 survey, and, according to the metadata, it is due to the presence of snow over the ground in a particular region which caused measurements in that area to be unreliable. The results show an excellent fit between the model prediction and the observations, and the ratios are extrapolated for all days until 2016-12-31, where the minimum value is approximately 0.14.

3.3. Spatial comparison for a specific temporal window

For a given temporal window, the decay corrected and gridded DOE and Safecast data are compared to estimate and remove bias. First, the error between each of the corresponding grid cells is computed, and then a transformation is applied to the Safecast data to minimize the error over all grid cells. In this paper, a simple statistical linear regressions is used to characterize the bias, which is assumed to be spatially uniform over the domain. This assumption seems to hold true for the FDNPP release, but other scenarios might require different

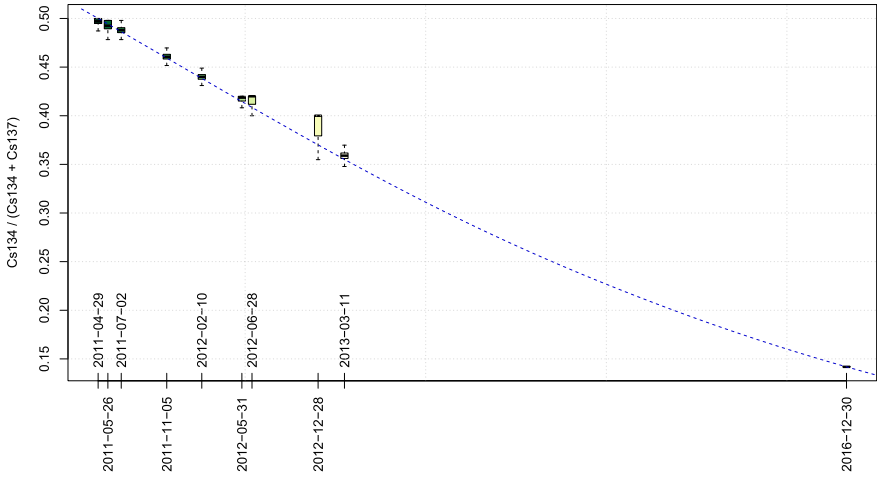

Fig. 6. Numerical prediction of the ratio of ^{134}Cs over (^{137}Cs + ^{134}Cs) as a function of time. The results from the nine field surveys are visualized with boxplots to show the distribution of the values over the domain.

transformations for each grid cell to account for a spatially dependent bias.

At each temporal window, a linear regression is used to predict the DOE data using the Safecast data as the input over all the grid cells. Generally, the Safecast data are consistently overestimating the DOE data, however, the transformation requires correcting both for an intercept (to account for the overestimation) and a slope (to account for different magnitude of errors between high and low values). The calibration model is applied to shift the Safecast data distribution in order to minimize the error between Safecast and DOE data. All computations are performed in logarithmic scale in order to not penalize low dose rates.

Linear regression identifies an intercept i and a slope s, which are added to and multiplied by the original Safecast measurements. While the analysis is performed over the gridded Safecast data, the transformation is applied to each individual measurement. Because each grid cell is the average of multiple values that can vary significantly, some of the values that are above background before being transformed can become below background after being transformed. For this reason, it is not possible to use the rasterized version of the data to apply this function, but it is necessary to transform each measurement individually and then consider the raster-based representation.

3.4. Time dependent model for data calibration

The steps described previously are performed for an extending temporal window with the same time period of origin but with a later end date. While the input DOE data are constant because they were acquired during a 2011 survey campaign, Safecast is a data stream that is constantly increasing in volume because they include measurements beginning in 2011 and continuing until the specified end date. Note, however, that while more data are available at later dates, it is not necessarily the case that a greater quantity of data are used in computations at later times. In fact, because dose rate measurements are being corrected for decay over time, all those measurements that when corrected for decay were below background at the later date were omitted. This is always true for the DOE data, since no new data are added and the number of valid grid cells monotonically decreases with time because measurements are corrected for decay to eventually be below the background radiation level and be removed from the analysis.

The regression coefficients identified during the multiple spatial comparisons performed are aggregated and interpolated using quadratic models for both slopes and intercepts. The result is a generalized model that can be used to calibrate the Safecast data as a function of time. The larger the number of temporal windows used, the higher the resolution of the new calibration coefficients. In this study, the interpolations were performed with a weekly cadence. This general model captures the trends of the Safecast bias over time, and it allows the calibration and validation of past data, but also, extrapolation to calibrate data for future observations.

4. Results and discussion

The methodology was applied to calibrate Safecast data from 2011 to 2016 over the domain of study. Each of the over six million Safecast measurements is first converted from cpm to μSv/h according to Equation (1), then adjusted by removing the background, and finally decay corrected using Equation (3) and the Cesium isotope ratio predicted (See Equation (4), Fig. 6 and Table 1). The decay corrected values are rasterized to the same common grid and then the background is added back. The rasterized DOE data are processed similarly by first removing the background, and then decay correcting each cell to the same date as for the Safecast data. This process is repeated for both DOE and Safecast data on a weekly basis between 2011 and 2016. In other words, the temporal windows that are used in this study start at the begin of the dataset and each assessment continually adds on an additional week of data. However, most results are presented only as an end of the year summary because of space constraints, and also because the weekly differences are very small.

As expected from the visualization of the overall Safecast data, their values are generally higher than the corresponding values in the DOE data. The (a) panels in Fig. 7 show the scatterplots for the two datasets for the temporal windows defined from the 2011-04-23 to the last day of 2011 (top three) and 2016 (bottom three). They show that the Safecast data are generally higher, and that this difference decreases with time. The hypothesis is that this over-estimation is due to an inconsistent conversion factor being used when converting the data acquired by the bGeigie instrument. In fact, as the Cesium isotopes decay, ^{134}Cs becomes negligible and only ^{137}Cs is present in detectable quantities, which is what the standard Safecast conversion factor is based upon.

The (b) panels in Fig. 7 show the data after being calibrated according to the coefficients of the linear fit at each temporal window. The results of the multiple regressions are shown in Fig. 8 in terms of the intercepts (left) and the slopes (right), which are both shown as a function of time. The results show a predictable pattern that is captured by using quadratic regressions (both shown with a dashed line). Table 2 shows the coefficients used to determine the slope and intercept to calibrate the Safecast data as a function of time, which is expressed both

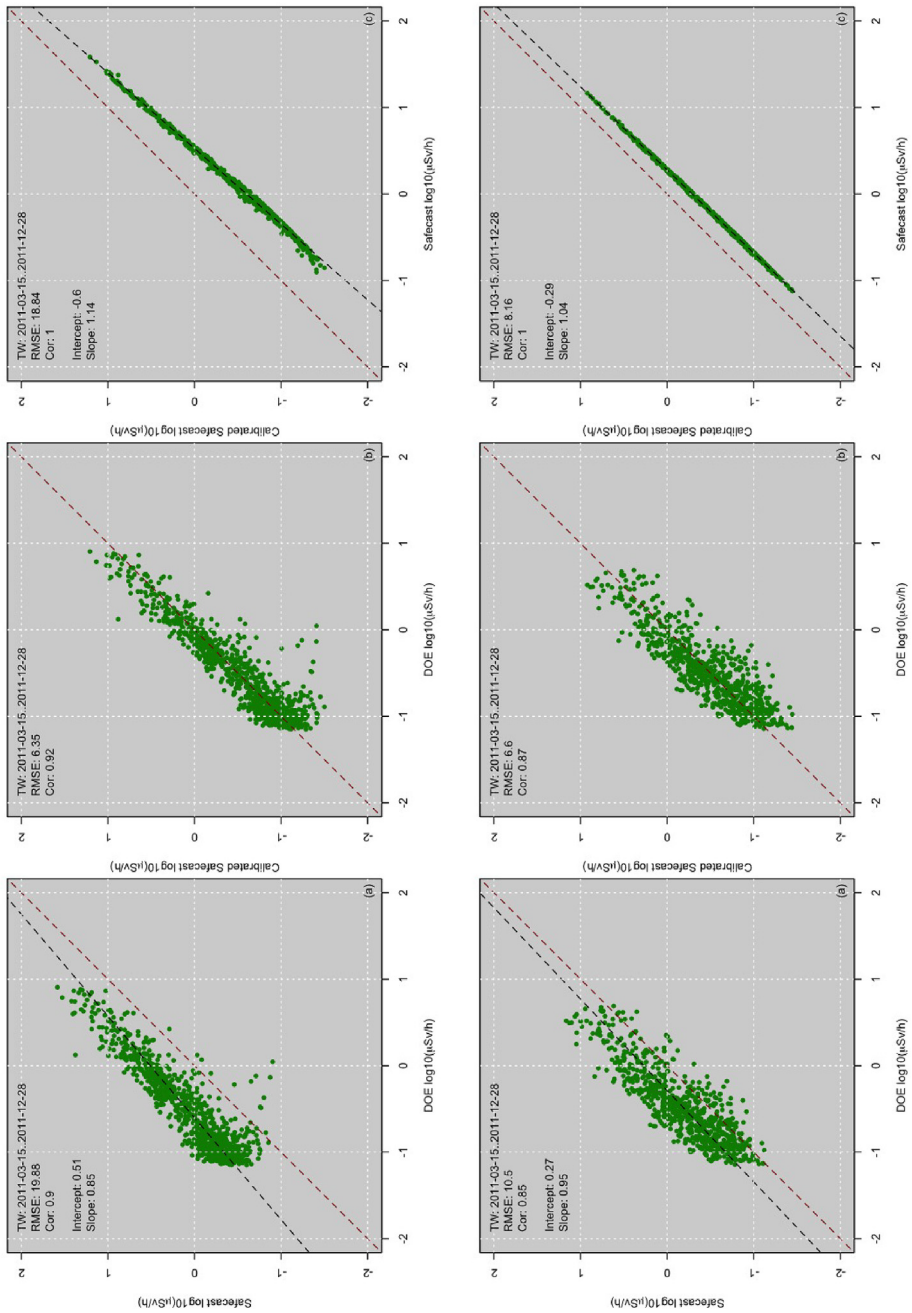

Fig. 7. Scatterplots comparing DOE and Safecast data for 2011 and 2011-2016. The (a) panels are the scatterplots for the data before transformation, and including the linear regressions performed. The (b) panels are the data after shifting the Safecast distribution according to the coefficients of the linear regression. The (c) panels are the scatterplots for the Safecast data before and after transformation, and including the linear regression to capture their relationship. All values are in μSv/h.

in the number of seconds since 1970-01-01 JST and elapsed fractional days since 2011-03-14. Both coefficients are given because the first can be used to easily calibrate Safecast data in the Fukushima area by using their official time stamps, while the second can be used as a general case where time is as a function of days from the initial release. This generalized model calibrates the Safecast data by applying a linear transformation to the M_t parameter in Equation (3). Therefore, the calibrated Safecast decay corrected value can be found by:

$$M_t^T = M_t \cdot S_t + I_t \tag{5}$$

$$\hat{D}^{tot}(M_t^T, R_t, \delta t) = (M_t^T \cdot (1 - R_t) \cdot D(\delta t, T_{1/2}^{137})) + (M_t^T \cdot R_t \cdot D(\delta t, T_{1/2}^{134})) \tag{6}$$

where S_t and I_t are respectively the slope and intercept at time t identified by multiple regression.

Each Safecast anomaly measurement (original measurement minus background) is transformed using Equation (5), thus generating a new calibrated dataset. These calibration coefficients can be extrapolated and applied to data beyond 2016, thus being crucial to calibrate future measurements. It is also to be noted, however, that future measurements require less correction since the contribution of ^{134}Cs is decreasing over time, and becomes negligible past 2020 (see Table 1). These coefficients are, however, also valid for eventual future releases where both Cesium isotopes are released in the environment. Furthermore, they permit Safecast data to be used as a reliable calibrated input for decision making.

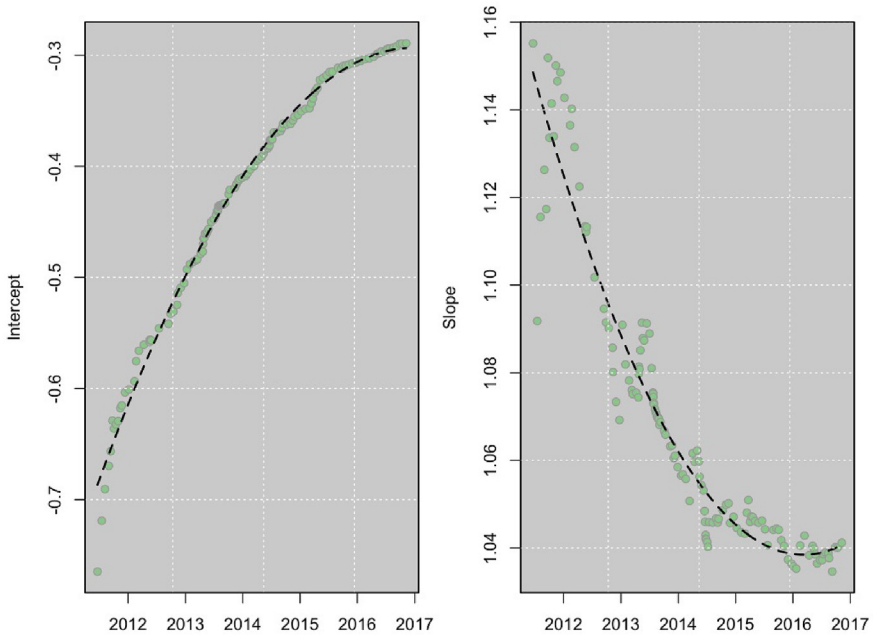

Fig. 8. Results of the different interpolations made on a weekly basis to calibrate Safecast and DOE data. The figure on the left shows the intercepts as a function of time, while the figure on the right shows the slopes as a function of time. The results of their fit is shown with a dashed line.

Table 2
Coefficients for the slope and intercept to calibrate Safecast data with respect to DOE data. The coefficients are given for Unix Time (UT) where t is the number of seconds since 1970-01-01 JST, and in Elapsed Time (ET) where t is the fractional number of days from the accident.

Parameter	Intercept	t	t^2
Slope (UT)	1.160e+01	−1.449e-08	4.970e-1
Intercept (UT)	−2.873e+01	3.835e-08	−1.293e-17
Slope (ET)	1.183e+00	−1.817e-04	5.549e-08
Intercept (ET)	−7.006e-01	3.610e-04	−7.811e-08

4.1. Validation

The calibrated Safecast data are gridded to the same common grid, and then compared to the DOE data. Fig. 9 show a comparison between the original Safecast data (left), the calibrated Safecast data (center), and the DOE data (right) for the temporal window from 2011-04-23 to the end of 2011 (top six panels) and 2016 (bottom six panels). The barplots are the distribution of the dose rates for the corresponding maps. Additionally, an overall error (RMSE) between the calibrated and uncalibrated Safecast and the DOE data were computed by taking the squared difference for each corresponding grid cell after transforming to Log10 scale, and by dividing by the number of valid grid cells.

In each case the spatial distribution of the calibrated Safecast and DOE data are much closer, both spatially and temporally, when compared with the uncalibrated Safecast data. Additionally, the barplots for the distribution of the radiation anomaly also show a higher correlation, and the absence of the higher values that are present in the uncalibrated Safecast data, and absent in the calibrated Safecast data. The RMSE was much lower between the calibrated Safecast and the DOE data. Thus the spatial and temporal distribution of the calibrated Safecast data are a good approximation of the DOE data. While the Safecast data contain several missing values along the footprint of the release, these data could be filled through spatial interpolation. In this study, however, data were not interpolated.

Although Fig. 9 shows results only for 2011 and 2011-2016, maps and associated errors were computed at a weekly cadence. The RMSE between uncalibrated and calibrated Safecast data with respect to the DOE data are shown in Fig. 10. Deviations from the DOE data are always smaller for the calibrated Safecast data. The error for calibrated Safecast data is quite flat, with a slight trend to increase with time. This trend is probably due to the decay corrected data containing few elevated but many small values, which skews the distribution before the linear interpolation.

4.2. Plume error comparison

An additional test was performed to compare the radiation distribution of the uncalibrated and calibrated Safecast data with respect to the DOE data along and across the direction of the main anomaly. This corresponds to the footprint of the plume starting at the FDNPP and spreading 20 km North-West. This test is important because it compares the data in the region where the risk to radiation exposure is highest. Therefore, the measurements used in this test from the plume are potentially the most useful and actionable during a emergency, but their collection poses a risk to the Safecast volunteers who could potentially be exposed to high levels of radiation.

In addition, a simulation was performed using a Gaussian reflected dispersion model, which predicts the mean concentration C_p at a location x, y, and z generated by a source located at x_s, y_s, and z_s as:

$$C_p(x, y, z, x_s, y_s, z_s) = \frac{Q g_y g_z}{2\pi U \left[\sigma_y^2 \sigma_z^2\right]^{1/2}} \tag{7}$$

with

$$g_y = \exp\left[-\frac{(y - y_s)^2}{2\sigma_y^2}\right]; \tag{8}$$

$$g_z = \exp\left[-\frac{(z - z_s)^2}{2\sigma_z^2}\right] + \exp\left[-\frac{(z + z_s)^2}{2\sigma_z^2}\right] \tag{9}$$

where Q is the mass emission rate, U is the wind speed, and $\sigma_y(x, x_s; \psi)$ and $\sigma_z(x, x_s; \psi)$ are the crosswind and vertical dispersion coefficients (i.e. the plume spreads) where ψ describes the atmospheric stability class (i.e., $\psi = A$ to $\psi = F$).

The values for Q, U were set to 6E13 μSv/h and 15 m/s respectively

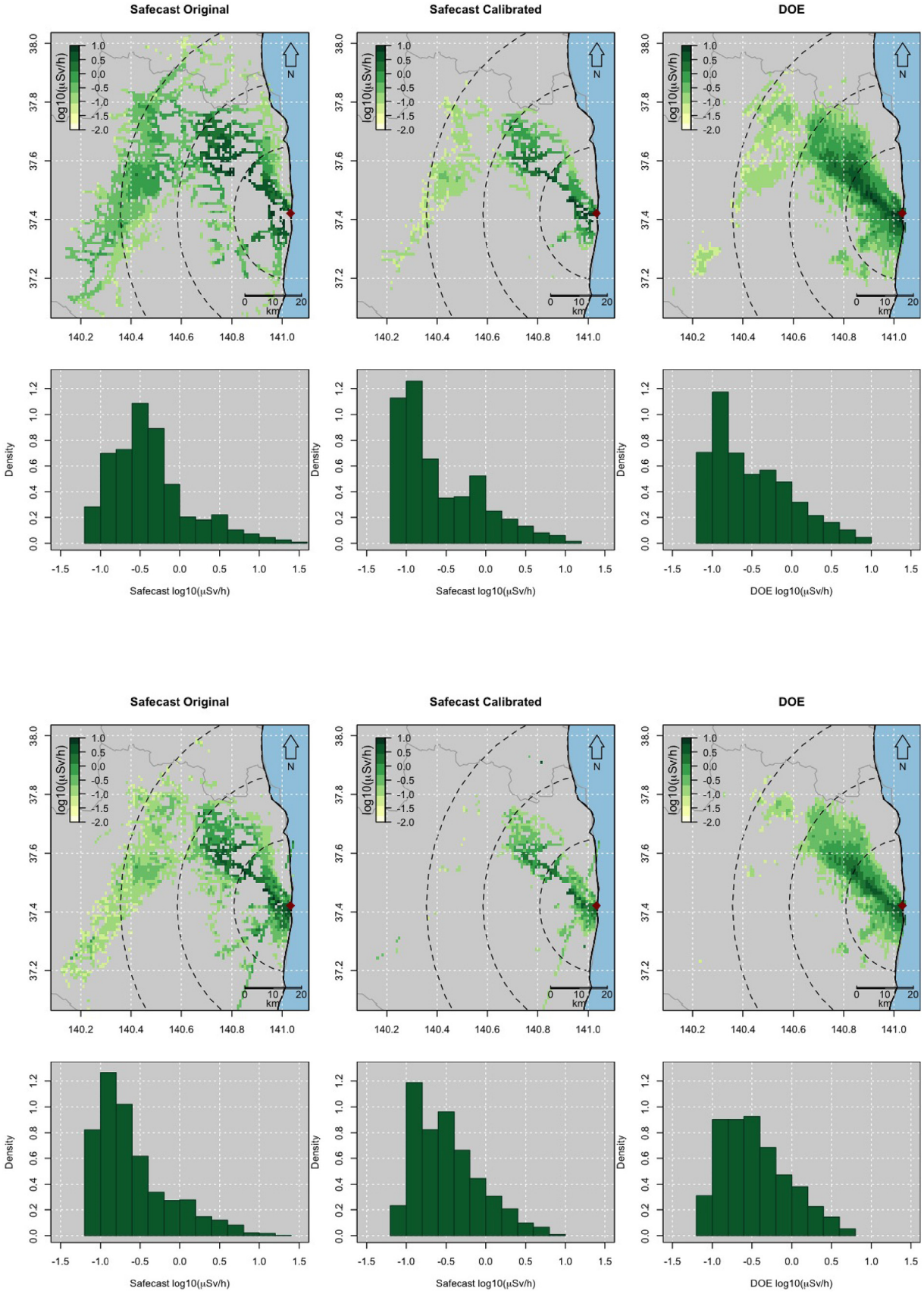

Fig. 9. Comparison between original Safecast data (left), calibrated Safecast data (center), and DOE data (right) for 2011 (top) and the same for 2011 through 2016 (bottom). The barplots show the distribution of the dose rates for the corresponding maps. All values are in μSv/h.

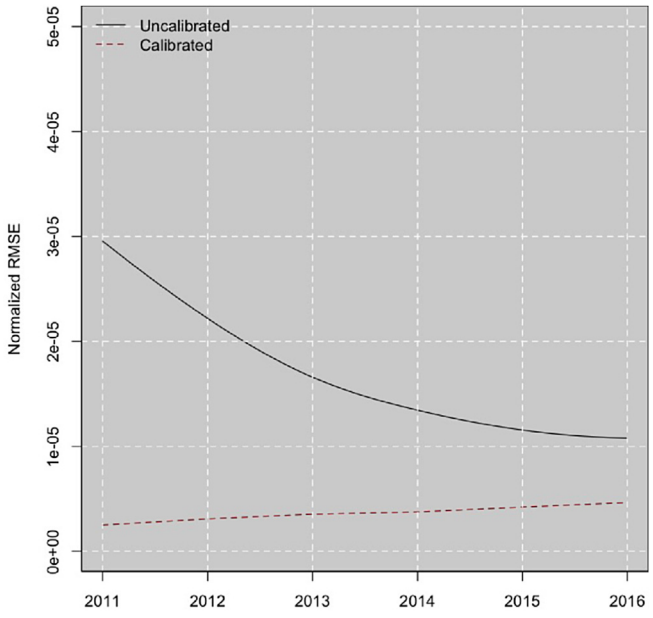

Fig. 10. Normalized Error between calibrated and uncalibrated Safecast data and DOE data.

(Cervone and Franzese, 2014). The dispersion coefficients ψ are computed from the tabulated curves of Briggs. The result of the simulation is the concentration field generated by the release along a wind direction θ, which in this case corresponds to 307° (clockwise from 0 pointing North). In the simulation the stability class ψ is set to E because it best matches the limited ground observations measured at the time of the accident at the airport in Fukushima.

Fig. 11 shows a comparison of the main anomaly for the uncalibrated Safecast data (a), calibrated data (b), the DOE data (c), and the Gaussian model (d) as of 2011-12-31. The locations of cross section (L1-L4 bottom to top) used to extract values are shown. The locations of the cross sections are specifically placed where the most data are present and, thus, allows for a more comprehensive comparison. Safecast data are collected primarily along roads which limits the spatial coverage of the dataset. The spatial density of the measurements are shown across the display of latitudes and longitudes of each panel. The figure shows that, as already discussed, the uncalibrated Safecast anomaly over-estimates the radiation, whereas the other datasets generally agree on the spatial distribution and magnitude of the anomaly. Additionally, it is also possible to see that the Gaussian model captures the overall distribution of the data, and it generally agrees with both DOE and calibrated Safecast data. It is important to remember that the Gaussian plume model can only model dispersion along a single wind direction.

Fig. 12 shows the dose rate measurements extracted along the cross sections L1 (a), L2 (b), L3 (c), and L4 (d) for the calibrated Safecast (solid green), uncalibrated Safecast (dashed green), DOE (black) and

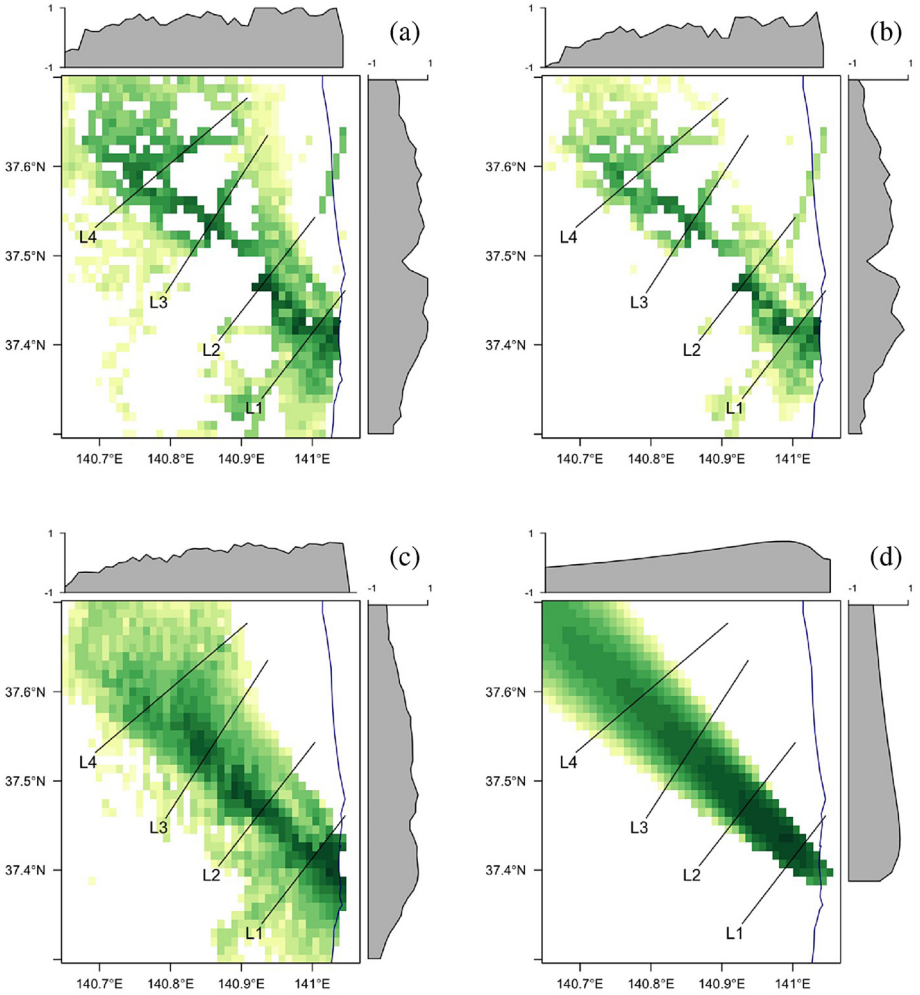

Fig. 11. Comparison of the main anomaly for the Safecast uncalibrated data (a), calibrated data (b), the DOE data (c), and the Gaussian model (d). Four cross section locations are shown as black lines and labeled L1-L4.

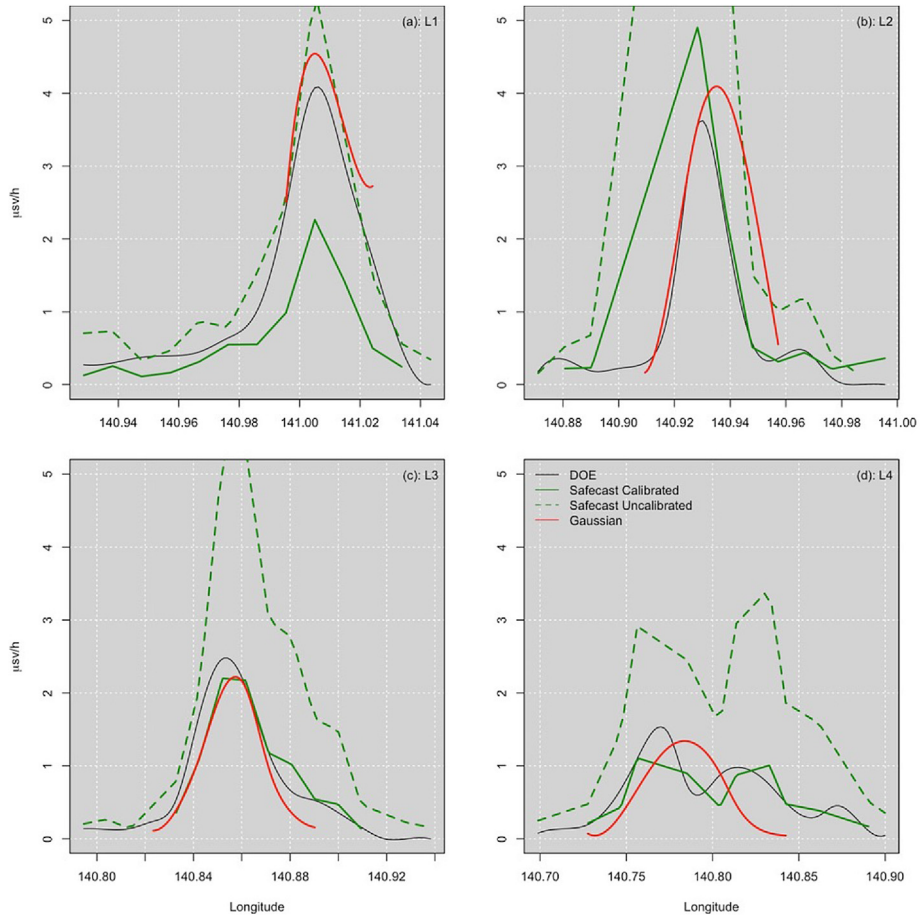

Fig. 12. Cross sections of dose rate measurements as a function of longitude for DOE, Safecast (both calibrated and uncalibrated), and the Gaussian model.

the Gaussian model (red). It is shown that, with the exception of uncalibrated Safecast, the datasets have very similar distributions across all four cross sections. It is concluded that the calibrated Safecast is a good estimator to reconstruct the DOE anomaly, and that a Gaussian plume model can be used to accurately approximate the anomaly. It is to be noted, however, that the simple reflected Gaussian model proposed cannot simulate the more complex geometry of the release past the initial 20 km.

5. Conclusions

This article presents a methodology to cross calibrate Safecast contributed dose rate measurements with DOE measurements taken after the 2011 radioactive releases at the FDNPP in Japan. Safecast measurements are collected continuously from 2011, and are compared with the official measurements taken in 2011 by taking into account their normal decay rates, missing values, and the spatial and temporal distributions. It is shown that calibrated Safecast data approximate the distribution of the U.S. government data, while uncalibrated data usually overestimate it.

A new set of calibration coefficients is presented which allows for the adjustment of the Safecast data and minimizes the deviations from the DOE measurement results. The coefficients are a function of time, and take into account the different ratios of ^{134}Cs and ^{137}Cs isotopes present in the environment. The ratio for the isotopes is modelled, and validated at nine dates when field studies are available. The failure to capture this ratio in the standard Safecast conversion is responsible for the systematic over-estimation of the contributed measurements when compared in µSv/h to the U.S. government measurements.

The new coefficients are expected to be valid until 2020, although, they might be slightly updated when Safecast data becomes available at later dates. It should be remembered, however, that because of the shorter half life of ^{134}Cs, the relative contribution of this isotope is diminishing over time. It is expected that the calibration coefficients for 2020 can be applied to all future data with only negligible errors being introduced.

The calibration coefficients are provided in terms of elapsed time from the initial release to be used as a general correction. They will allow Safecast data to be used during emergency situations for decision making by providing a well calibrated dataset that should closely approximate results from airborne measurements by DOE. Models developed to use DOE data as an input can use the contributed data by applying the calibration described in this paper.

Acknowledgements

This research was funded by ONR grant N00014-14-1-0208. This research was primarily conducted at the National Center for Atmospheric Research.

Appendix A. Supplementary data

Supplementary data related to this article can be found at http://dx.doi.org/10.1016/j.jenvrad.2018.04.018.

References

Bowyer, T.W., Biegalski, S.R., Cooper, M., Eslinger, P.W., Haas, D., Hayes, J.C., Miley, H.S., Strom, D.J., Woods, V., 2011. Elevated radioxenon detected remotely following the Fukushima nuclear accident. J. Environ. Radioact. 102 (7), 681–687.
Brown, A., Franken, P., Bonner, S., March 2016a. The Safecast Report.

Brown, A., Franken, P., Bonner, S., Dolezal, N., Moross, J., 2016b. Safecast: successful citizen-science for radiation measurement and communication after Fukushima. J. Radiol. Prot. 36 (2), S82.
Calabrese, E., 2011. Improving the scientific foundations for estimating health risks from the Fukushima incident. Proc. Natl. Acad. Sci. Unit. States Am. 108 (49), 19447–19448.
Cervone, G., Franzese, P., 2014. Source term estimation for the 2011 Fukushima nuclear accident. In: Data Mining for Geoinformatics. Springer, pp. 49–64.
Cervone, G., Sava, E., Huang, Q., Schnebele, E., Harrison, J., Waters, N., 2016a. Using twitter for tasking remote-sensing data collection and damage assessment: 2013 Boulder flood case study. Int. J. Rem. Sens. 37 (1), 100–124.
Cervone, G., Schnebele, E., Waters, N., Moccaldi, M., Sicignano, R., 2016b. Using social media and satellite data for damage assessment in urban areas during emergencies. In: Seeing Cities through Big Data. Springer, pp. 443–457.
Coletti, M., Hultquist, C., Kennedy, W.G., Cervone, G., 2017. Validating safecast data by comparisons to a us department of energy Fukushima prefecture aerial survey. J. Environ. Radioact. 171, 9–20.
Department of Energy, 2011. US DOE/NNSA Response to 2011 Fukushima Incident- Raw Aerial Data and Extracted Ground Exposure Rates and Cesium Deposition.
Fairbairn, D., Al-Bakri, M., 2013. Using geometric properties to evaluate possible integration of authoritative and volunteered geographic information. ISPRS Int. J. Geo-Inf. 2, 349–370.
Fast, V., Rinner, C., 2014. A systems perspective on volunteered geographic information. ISPRS Int. J. Geo-Inf. 3, 1278–1292.
Fowler, A., Whyatt, J.D., Davies, G., Ellis, R., 2013. How reliable are citizen-derived scientific data? Assessing the quality of contrail observations made by the general public. Trans. GIS 17 (4), 488–506.
Goodchild, M., 2007. Citizens as sensors: the world of volunteered geography. Geojournal 69 (4), 211–221.
Hemmi, A., Graham, I., 2014. Hacker science versus closed science: building environmental monitoring infrastructure. Information Commun. Soc. 17 (7), 830.
Hultquist, C., Cervone, G., 2017. Citizen monitoring during hazards: validation of Fukushima radiation measurements. Geojournal 1–18.
Japan Atomic Energy Agency, 2014. Airborne Monitoring in the Distribution Survey of Radioactive Substances.
Katata, G., Ota, M., Terada, H., Chino, M., Nagai, H., 2012. Atmospheric discharge and dispersion of radionuclides during the Fukushima Dai-ichi Nuclear Power Plant accident. Part I : source term estimation and local-scale atmospheric dispersion in early phase of the accident. J. Environ. Radioact. 109, 103–113.
Kinoshita, N., Sueki, K., Sasa, K., Kitagawa, J., Ikarashi, S., Nishimura, T., Wong, Y., Satou, Y., Handa, K., Takahashi, T., et al., 2011. Assessment of individual radionuclide distributions from the Fukushima nuclear accident covering central-east Japan. Proc. Natl. Acad. Sci. Unit. States Am. 108 (49), 19526–19529.
Lyons, C., Colton, D., 2012. Aerial measuring system in Japan. Health Phys. 102 (5), 509–515.
Masson, O., Baeza, A., Bieringer, J., Brudecki, K., Bucci, S., Cappai, M., Carvalho, F., Connan, O., Cosma, C., Dalheimer, A., et al., 2011. Tracking of airborne radionuclides from the damaged Fukushima Daiichi nuclear reactors by european networks. Environ. Sci. Technol. 45 (18), 7670–7677. http://dx.doi.org/10.1021/es2017158.
Morino, Y., Ohara, T., Nishizawa, M., 2011. Atmospheric behavior, deposition, and budget of radioactive materials from the Fukushima Daiichi nuclear power plant in march 2011. Geophys. Res. Lett. 38 (7).
Potiriadis, C., Kolovou, M., Clouvas, A., Xanthos, S., 2011. Environmental Radioactivity Measurements in Greece Following the Fukushima Daichi Nuclear Accident. Radiation Protection Dosimetry to Appear. Radiat. Protect. Dosim. Appear 150 (4), 441–447.
Safecast, December 2015a. About Calibration and the Bgeigie Nano.
Safecast, December 2015b. Bgeigie Nano Kit.
Safecast, December 2016. About Safecast.
Saito, K., Tanihata, I., Fujiwara, M., Saito, T., Shimoura, S., Otsuka, T., Onda, Y., Hoshi, M., Ikeuchi, Y., Takahashi, F., Kinouchi, N., Saegusa, J., Seki, A., Takemiya, H., Shibata, T., 2015. Detailed deposition density maps constructed by large-scale soil sampling for gamma-ray emitting radioactive nuclides from the Fukushima dai-ichi nuclear power plant accident. J. Environ. Radioact. 139, 308–319.
Spinrad, P., 25 April, 2011. John Iovine: Geiger Counter Sanity Check. Makezine.
Sprake, J., Rogers, P., 2014. Crowds, citizens and sensors: process and practice for mobilising learning. Personal Ubiquitous Comput. 18 (3), 753–764.
Stohl, A., Seibert, P., Wotawa, G., Arnold, D., Burkhart, J., Eckhardt, S., Tapia, C., Vargas, A., Yasunari, T., 2012. Xenon-133 and caesium-137 releases into the atmosphere from the Fukushima Dai-ichi nuclear power plant: determination of the source term, atmospheric dispersion, and deposition. Atmos. Chem. Phys. 12 (5), 2313–2343.
Terada, H., Katata, G., Chino, M., Nagai, H., Oct. 2012. Atmospheric discharge and dispersion of radionuclides during the Fukushima Dai-ichi Nuclear Power Plant accident. Part II: verification of the source term and analysis of regional-scale atmospheric dispersion. J. Environ. Radioact. 112, 141–154.
Yasunari, T., Stohl, A., Hayano, R., Burkhart, J., Eckhardt, S., Yasunari, T., 2011. Cesium-137 deposition and contamination of Japanese soils due to the Fukushima nuclear accident. Proc. Natl. Acad. Sci. Unit. States Am. 108 (49), 19530–19534.